Membrane Location of Spin-Labeled M13 Major Coat Protein Mutants Determined by Paramagnetic Relaxation Agents†

David Stopar,‡,§ Kitty A. J. Jansen,‡ Tibor Páli,||,⊥ Derek Marsh,*,|| and Marcus A. Hemminga*,‡

Department of Molecular Physics, Agricultural University, Dreijenlaan 3, NL-6703 HA Wageningen, The Netherlands, and Max-Planck-Institut für biophysikalische Chemie, Abteilung Spektroskopie, D-37077 Göttingen, Germany

Received January 22, 1997; Revised Manuscript Received April 14, 1997⊗

ABSTRACT: Mutants of the M13 bacteriophage major coat protein containing single cysteine replacements (A25C, V31C, T36C, G38C, T46C, and A49C) in the hydrophobic and C-terminal domains were purified from viable phage. These were used for site-directed spin-labeling to determine the location and assembly of the major coat protein incorporated in bilayer membranes of dioleoylphosphatidylcholine. The membrane location of the spin-labeled cysteine residues was studied with molecular oxygen and Ni^{2+} ions as paramagnetic relaxation agents preferentially confined to the hydrophobic and aqueous regions, respectively, by using progressive-saturation electron spin resonance (ESR) spectroscopy. The section of the protein around Thr36 is situated at the center of the membrane. Residue Thr46 is placed at the membrane surface in the phospholipid head group region with a short C-terminal section, including Ala49, extending into the aqueous phase. Residue Ala25 is then positioned consistently in the head group region of the apposing lipid monolayer leaflet. These positional assignments are consistent with the observed mobilities of the spin-labeled groups. The outer hyperfine splittings in the ESR spectra decrease from the N-terminal to the C-terminal of the hydrophobic section (residues 25−46), and then drop abruptly in the aqueous phase (residue 49). Additionally, the strong immobilization and low oxygen accessibility of residue 25 are attributed to steric restriction at the hinge region between the transmembrane and N-terminal amphipathic helices. Sequence-specific modulations of the ESR parameters are also observed. Relatively low oxygen accessibilities in the hydrophobic region suggest intermolecular associations of the transmembrane helices, in agreement with saturation transfer ESR studies of the overall protein mobility. Relaxation enhancements additionally reveal a Ni^{2+} binding site in the N-terminal domain that is consistent with a surface orientation of the amphipathic helix.

The major coat protein of bacteriophage M13 exists, prior to phage assembly, as a small monotopic integral protein in the plasma membrane of the *Escherichia coli* host cell. The major coat protein has a hydrophobic stretch of 20 amino acids, flanked by an acidic N-terminal region located in the periplasm and a basic C-terminal region located in the cytoplasm (Asbeck et al., 1969). The overall secondary structure of the protein is α-helical with a turn structure between Gly23 and Glu20. This specific β-turn connects the transmembrane helix with an amphipathic N-terminal helix. Although the secondary structure of the protein is well characterized (McDonnell et al., 1993; Van de Ven et al., 1993), the location of the secondary structural elements relative to the lipid bilayer is poorly identified. In this paper, the emphasis is placed on the membrane location of the transbilayer helix and of the C-terminal domain of the protein, where the presence of four positively charged lysines intercalated between hydrophobic residues complicates the positioning relative to the membrane−water interface (Turner & Weiner, 1993).

To obtain information on the location of the membrane-bound form of the major coat protein and in particular of the C-terminal domain, a series of site-specific cysteine mutants were prepared for studies using electron spin resonance (ESR)[1] spectroscopy. Such an approach allows site-directed spin-labeling at specific residue attachment sites (Altenbach et al., 1989). Care is required, however, in the design of the mutations in order to avoid nonfunctional proteins. Mutations of the M13 major coat protein prepared here did not include replacement of any charged or aromatic residues which apparently causes lethal mutations (Marvin et al., 1994). Selection for viable mutant bacteriophages ensured the choice of functional mutant major coat proteins. Purified mutant major coat proteins were spin-labeled and incorporated in phospholipid bilayers as model integral membrane proteins.

† This research was supported by the Slovenian Ministry of Science and Technology.

* Authors to whom correspondence should be addressed at the Department of Molecular Physics, Agricultural University, P.O. Box 8128, NL-6700 ET Wageningen, The Netherlands (M.A.H.), and at the Abteilung Spektroskopie, Max-Planck-Institut für biophysikalische Chemie, Am Fassberg, D-37077 Göttingen, Germany (D.M.)

‡ Agricultural University.

§ Permanent address: University of Ljubljana, Biotechnical Faculty, Vecna pot 111, SL-61000 Ljubljana, Slovenia.

|| Max-Planck-Institut für biophysikalische Chemie.

⊥ Permanent address: Institute of Biophysics, Biological Research Centre, H-6701 Szeged, Hungary.

⊗ Abstract published in *Advance ACS Abstracts,* June 15, 1997.

[1] Abbreviations: DOPC, 1,2-dioleoyl-*sn*-glycero-3-phosphocholine; TS, 4-octadecanoyl-2,2,6,6-tetramethylpiperidine-*N*-oxyl; DTNB, 5,5′-dithiobis(2-nitrobenzoic acid); L/P, lipid to protein molar ratio; 5-MSL, 3-maleimido-2,2,5,5-tetramethylpyrrolidine-*N*-oxyl; *n*-PCSL, 1-acyl-2-[*n*-(4,4-dimethyloxazolidine-*N*-oxyl)stearoyl]-*sn*-glycero-3-phosphocholine; *n*-SASL, *n*-(4,4-dimethyloxazolidine-*N*-oxyl)stearic acid; SDS, sodium dodecyl sulfate; ESR, electron spin resonance; ST-ESR, saturation transfer electron spin resonance; HPSEC, high-performance size-exclusion chromatography; rpm, rotations per minute.

S0006-2960(97)00139-6 CCC: $14.00

The position of the spin-label on the protein in the membrane-bound form was determined from the interaction of the nitroxide label with paramagnetic relaxation agents by using progressive saturation ESR spectroscopy (Páli et al., 1993; Snel et al., 1994). Combination with site-directed spin-labeling generally allows one to obtain detailed information on the secondary and tertiary protein structure (Hubbell et al., 1996). The relaxation agents, molecular oxygen and paramagnetic ions, were used earlier to determine the location and immersion depth in the membrane of specific spin-labeled sites in bacteriorhodopsin, apocytochrome *c*, and cytochrome *c* (Altenbach et al., 1990, 1994; Snel et al., 1994). Changes in the nitroxide spin−lattice relaxation rates on interaction with fast-relaxing paramagnetic species are a measure of their accessibility or distance of closest approach to the nitroxide group (Páli et al., 1992). Oxygen dissolves preferentially in the hydrophobic core of the membrane, whereas uncomplexed paramagnetic ions are restricted mainly to the aqueous phase (Subczynski & Hyde, 1983, 1984). A relatively low accessibility to oxygen is, however, not entirely diagnostic for the spin-label location, because it may arise either from exposure of the label to the aqueous phase or from the label being buried in the interior of the protein (Altenbach et al., 1990). In the later case, a range of values may be expected depending on the protein environment. Thus, a combination of relaxation data from both oxygen and a paramagnetic ion is required for unambiguous interpretation in terms of the protein topography (Marsh, 1994).

In the present work, the location of the spin-labeled M13 coat protein cysteine mutants was determined with Ni^{2+} ions and oxygen as relaxation agents in lipid bilayers of dioleoylphosphatidylcholine. This was calibrated by using similar measurements on specific positionally spin-labeled lipids (*n*-PCSL and TS) in the same lipid bilayer system.

MATERIALS AND METHODS

Materials. DOPC was obtained from Avanti Polar Lipids (Birmingham, AL). Spin-labeled phosphatidylcholine derivatives (*n*-PCSL) were synthesized from the corresponding stearic analogues (*n*-SASL) specifically spin-labeled at different positions in the *sn*-2 chain as described previously (Marsh & Watts, 1982). The tempol ester of stearic acid (TS) spin-label was obtained from Molecular Probes (Eugene, OR). 5-Maleimidoproxyl (5-MSL) and DTNB (Ellman's reagent) were obtained from Sigma (St. Louis, MO).

Lipid Vesicle Preparation. Lipid vesicles were prepared by dissolving 1 mg of DOPC and 1 mol % spin-labeled lipid in chloroform/methanol (2:1, v/v) solvent. To prevent peroxidation of the unsaturated lipid chains, 0.1 mol % butylated hydroxytoluene was added to the lipid solution. The solvent was evaporated with nitrogen gas, and residual traces of solvent were removed by drying under vacuum overnight. Lipids were hydrated with 100 μL of oxygen-saturated buffer (150 mM NaCl, 10 mM Tris-HCl, pH 7.0), or deoxygenated buffer containing 0, 5, 10, 25, or 50 mM $NiCl_2$, by vortex mixing at room temperature.

Major Coat Protein Spin-Labeling. Six M13 major coat protein cysteine mutants (A25C, V31C, T36C, G38C, T46C, and A49C) with a yield high enough for ESR purposes were grown and purified from phage as described previously (Spruijt et al., 1989; Stopar et al., 1996). Major coat protein mutants were spin-labeled with 5-maleimidoproxyl spin-label (5-MSL), directly after bacteriophage disruption. Typically 5−10 mg of bacteriophage was suspended in 100 mM sodium cholate, 150 mM NaCl, 10 mM Tris-HCl, pH 7.0, with subsequent addition of 2.5% (v/v) chloroform. The mixture was incubated at 37 °C for 10 min with occasional mixing. To remove chloroform, the mixture was flushed with nitrogen gas until a clear nonopalescent suspension was obtained. To this suspension was added a 3-fold molar excess of 5-MSL spin-label, and the mixture was incubated for 30 min at 37 °C. The reaction was stopped by addition of excess cysteine. The mixture was applied to a HiPrep 16/60 Sephacryl S-300 High Resolution column (Pharmacia, Uppsala, Sweden), that was eluted with 25 mM sodium cholate, 150 mM NaCl, and 10 mM Tris-HCl, pH 7.0, to separate the major coat protein from DNA and free spin-label. Fractions with an A_{280}/A_{260} absorbance ratio higher than 1.4 were collected and concentrated by Amicon filtration. Before storage at 4 °C, sodium cholate was added to a final concentration of 50 mM.

Labeling Efficiency. The extent of spin-labeling was determined by using the reaction with DTNB to assay remaining free sulfhydryl groups. A bacteriophage suspension (2 mg/mL) was disrupted, and an aliquot was labeled as described above in 100 mM sodium cholate, 150 mM NaCl, 10 mM Tris-HCl, pH 7.0. The control unlabeled sample was disrupted in the same buffer and incubated for 30 min at 37 °C. To determine the amount of free cysteine groups after spin-labeling, 100 μL of DTNB stock solution (4 mg/mL in sodium phosphate buffer, pH 8.0) was added to 900 μL of spin-labeled or control unlabeled major coat protein suspension and incubated for 15 min at room temperature. The degree of labeling of the wild-type protein has been discussed in an earlier paper (Stopar et al., 1996) and is not significant compared to the specific labeling under the conditions used (30 min, pH 7.0). The absorption at 412 nm was determined for the spin-labeled mutant and control samples, and the percentage of labeled SH groups relative to the control sample was calculated.

Coat Protein Reconstitution in Lipid Vesicles. Incorporation of the spin-labeled major coat protein mutants into DOPC vesicles was performed from dispersions in sodium cholate as described earlier (Spruijt et al., 1989), with the following modifications. Lipid vesicles were prepared by dissolving the desired amount of DOPC in chloroform/methanol (2:1, v/v). To prevent lipid peroxidation, 0.1% (mol/mol) butylated hydroxytoluene was added to the solution. The solvent was evaporated with a stream of nitrogen gas, and the samples were dried under vacuum overnight to remove residual traces of the solvent. The lipids were solubilized in 50 mM sodium cholate buffer (150 mM NaCl, 10 mM Tris-HCl, pH 7.0) by sonication for 1 min (Sonifier cell disrupter, Model W185, Heat Systems-Ultrasonics Inc.). The desired amount of spin-labeled mutant major coat protein was added to give a lipid/protein molar ratio of 50 (L/P 50). Dialysis was performed at room temperature against a 100-fold excess of deoxygenated buffer (150 mM NaCl, 10 mM Tris-HCl, pH 7.0). The dialysis buffer was changed 4 times every 12 h. After dialysis, the proteoliposome suspension either was adjusted to the desired $NiCl_2$ concentration (0, 0.5, 1, 2.5, 5, 10, 15 or 25 mM $NiCl_2$, 150 mM NaCl, 10 mM Tris-HCl, pH 7.0) in deoxygenated buffer or was saturated with oxygen. The proteoliposomes were concen-

trated by centrifugation (Beckman L7-55 ultracentrifuge, 45 000 rpm, 2.5 h, 10 °C). To ensure accessibility of Ni^{2+} to all lipid membrane surfaces, the samples containing various concentrations of $NiCl_2$ were freeze-dried and then resuspended in a volume of distilled water equal to that of the original dispersion before preparing the samples for ESR measurements. Freeze-drying and resuspension did not alter the spectra in the absence of Ni^{2+} or oxygen as compared to the non-freeze-dried samples (data not shown).

The aggregation state of the major coat protein mutants in the reconstituted membrane samples was checked by using high-performance size-exclusion chromatography (HPSEC) (Spruijt et al., 1989). The L/P ratios and homogeneity of the samples were determined directly after sample preparation as described previously (Spruijt et al., 1989).

ESR Spectroscopy. Membrane dispersions were loaded into glass capillaries (i.d. 1 mm), flushed with oxygen or argon as required, and were pelleted at 12 000 rpm for 10 min in a Biofuge A. Excess supernatant was removed from the pellets in the ESR capillaries to obtain samples 5 mm in length. This avoids inhomogeneities of the microwave and modulation fields in the ESR cavity (Fajer & Marsh, 1982). The sample capillary was flushed with either argon or oxygen and sealed with a fine-wire thermocouple inserted directly into the sample. ESR spectra were recorded on a Varian Century Line Series 9 GHz spectrometer equipped with a nitrogen gas-flow temperature regulation system. The spectrometer was interfaced to an IBM PC for digital data collection. The sample capillaries were accommodated within standard 4 mm quartz ESR tubes containing light silicone oil for thermal stability. Conventional first harmonic, in-phase, absorption spectra were recorded at a modulation frequency of 100 kHz and modulation amplitude of 0.05 mT, and microwave amplitudes ranging from 0.0002 to 0.06 mT for progressive saturation measurements. The microwave amplitudes were measured as described in Fajer and Marsh (1982). Low-power conventional ESR spectra were recorded at a subsaturating microwave amplitude of $B_1 = 8.3\ \mu$T for line shape analysis. ST-ESR spectra were recorded in the second harmonic, 90° out-of-phase absorption mode at a modulation frequency of 50 kHz, a modulation amplitude of 0.5 mT, and an average microwave field $\langle B_1^2\rangle^{1/2}$ of 0.025 mT, according to the standardized protocol for dealing with cavity Q variations and field inhomogeneities (Fajer & Marsh, 1982; Hemminga et al., 1984). The phase was set using the self-null method (Marsh, 1981) at a subsaturating microwave field. Effective rotational correlation times were determined from the diagnostic line height ratios in the ST-ESR spectra, as described in Horváth and Marsh (1983). First and second integrals of ST-ESR and conventional ESR spectra, respectively, were determined after a base line correction.

Evaluation of Relaxation Rates. For labels with anisotropic line shapes (5- and 9-PCSL and all spin-labeled mutants except A49C), convolutions of Lorentzian and Gaussian functions, i.e., Voigt absorption line shapes, were fitted simultaneously to the low- and high-field wings of the low- and high-field peaks in the low-power unsaturated conventional ESR spectra, after the center of each line was determined. Fitting parameters were the Lorentzian line width and vertical normalization for the two lines, and a common Gaussian line width. This procedure corrects for the inhomogeneous line broadening, yielding the homogeneous (i.e., Lorentzian) line widths for both lines (Bales, 1989). For labels with isotropic line shapes (TS, 14-PCSL, and spin-labeled mutant A49C), the low-power conventional ESR spectra were first integrated with respect to magnetic field and then fitted to a sum of three Voigt absorption line shapes. The Lorentzian line widths were used to calculate the spin−spin relaxation times T_{2L}, T_{2C}, and T_{2H} for the low-field, central, and high-field hyperfine manifolds, respectively. For the anisotropic line shapes, it was assumed that $T_{2C} \approx T_{2L}$.

In the progressive saturation experiments, the second integral of the first-derivative absorption spectra (i.e., the spectral intensity of absorption), I, was determined as a function of the microwave amplitude, B_1. These values were fitted to the following dependence on B_1:

$$I(B_1) = I_0 B_1 \left[\frac{1}{\sqrt{1 + \gamma^2 B_1^{\,2} T_1 T_{2L}}} + \frac{1}{\sqrt{1 + \gamma^2 B_1^{\,2} T_1 T_{2C}}} + \frac{1}{\sqrt{1 + \gamma^2 B_1^{\,2} T_1 T_{2H}}} \right] \quad (1)$$

where T_{2L}, T_{2C}, and T_{2H} were the spin−spin relaxation times determined from the line widths and γ is the electron gyromagnetic ratio (Páli et al., 1993). The two fitting parameters were the spin−lattice relaxation time, T_1, and a common normalization factor, I_0. Equation 1 describes the saturation of the integrated intensity of the three hyperfine components in the absence of cross-relaxation, nuclear relaxation, and spin-exchange processes (Marsh, 1995a,b). The above procedure results in determinations of T_1 that are far less sensitive to inhomogeneous broadening than are standard amplitude or line width saturation techniques for measuring T_1T_2 products (Páli et al., 1993).

Accessibility Parameters. In the presence of a fast-relaxing paramagnetic species, the spin−lattice relaxation rate, $1/T_1$, of the spin-label is enhanced by an amount depending on the concentration, c, of the fast-relaxing species (Snel & Marsh, 1993):

$$1/T_1 = 1/T_1^{\,0} + k_{RL}c \quad (2)$$

Here T_1^0 is the value of T_1 for $c = 0$, and k_{RL} is an accessibility parameter that depends on the diffusion coefficient and cross section for collision of the relaxing agents in the case of Heisenberg spin exchange, and on the distance of closest approach to the spin-label in the case of magnetic dipole−dipole interactions (Marsh, 1994).

In the case of molecular oxygen, the accessibility parameter is defined as the difference in the T_1 relaxation rate for the nitroxide group in the presence (p) and in the absence (o) of a paramagnetic species:

$$\text{accessibility parameter} = 1/T_1^{\,p} - 1/T_1^{\,o} \quad (3)$$

For oxygen, the exchange interaction with spin-labels is assumed to be diffusion-controlled, and is determined by the local concentration of oxygen in the vicinity of the spin-label (Subczynski & Hyde, 1984).

RESULTS

The mutant coat proteins were indistinguishable from the wild-type protein with respect to their aggregational state

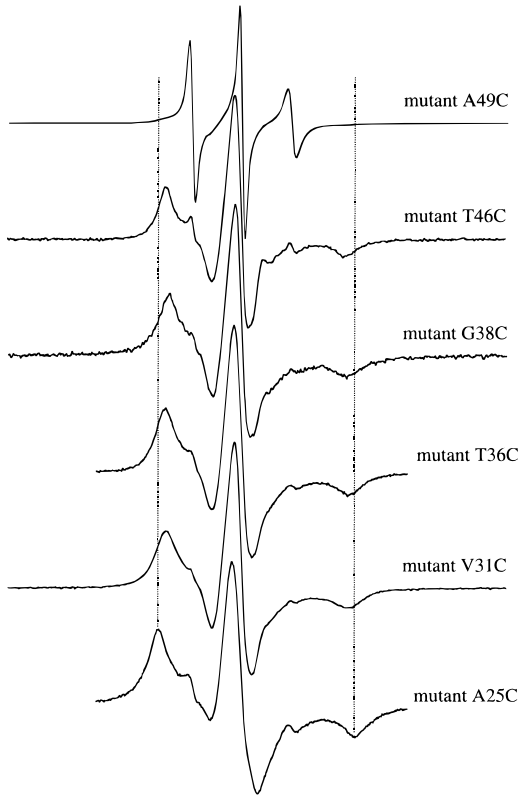

FIGURE 1: Conventional ESR spectra of spin-labeled major coat protein mutants in DOPC bilayers at a lipid/protein ratio 50 mol/mol. Spectra are normalized to the same central line height. The temperature of the samples is 20 °C. Total scan width is 16 mT for the spin-labeled mutants A49C, T46C, G38C, and V31C and 10 mT for the spin-labeled mutant coat proteins T36C and A25C.

and conformational state in reconstituted systems, as has been described previously (Stopar et al., 1996). The HPSEC elution profiles indicated that all the mutant proteins, except for mutant G38C, were in an α-helical oligomeric form, with no β-sheet polymeric form. The mutant G38C had a tendency to form β-sheet polymers under the experimental conditions used for reconstitution (up to 50% β-sheet conformation). For all cysteine mutants, the formation of S−S-bridged dimers immediately after phage disruption was less than 5%.

The spin-labeling efficiency in 100 mM sodium cholate buffer was 90% (±5%) for the mutant coat protein A25C, 88% (±5%) for the mutant V31C, 50% (±5%) for the mutant T36C, 77% (±5%) for the mutant G38C, 93% (±5%) for the mutant T46C, and 97% (±2.5%) for the mutant A49C. The residue positions 36 and 38 are significantly less accessible for alkylation by the maleimide spin-label than are the other positions.

The conventional ESR spectra of the various 5-MSL spin-labeled coat protein mutants, incorporated in DOPC bilayers at L/P 50 mol/mol, are given in Figure 1. The spectra are characteristic of one of two different motional regimes sensed by the different spin-labels: fast for the spin-labeled A49C mutant or slow for the spin-labeled T46C, G38C, T36C, V31C, and A25C mutants. This is consistent with an extramembranous location of residue 49 and a membrane location of the other residues, as will be discussed below. The outer hyperfine splitting in the spectra of the nitroxide radicals varies along the protein primary sequence, but the overall shape of the spectra is not influenced by the presence

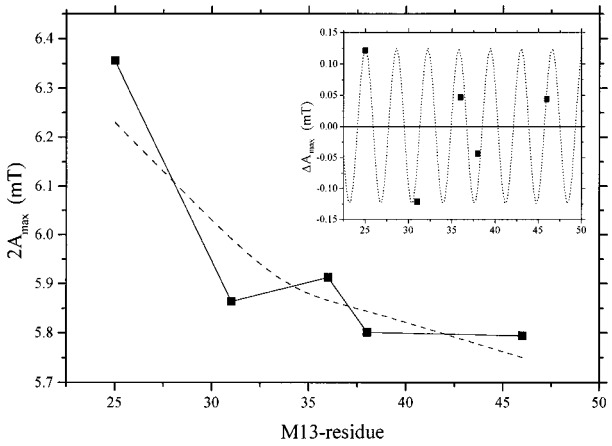

FIGURE 2: Dependence of the outer hyperfine splitting, $2A_{max}$, on spin-labeled residue position for cysteine mutants of the M13 major coat protein in DOPC bilayers at 20 °C. The dashed line connects the mean splittings between successive measurement points. The inset shows the deviation of A_{max} from the local mean value, with an α-helical periodicity superimposed (dotted line).

of $NiCl_2$ or oxygen relaxation agents. The positional dependence of the outer hyperfine splitting, $2A_{max}$, for those labels that give immobilized ESR spectra is presented in Figure 2. Overall, the outer hyperfine splitting decreases on going from the N-terminal to the C-terminal in this section of the protein (dashed line in Figure 2 and figure legend), but with a local sequence-specific periodicity superimposed (see inset to Figure 2). Although the total number of measurement points is limited by the requirement that all cysteine mutants used should assemble in viable phage, there clearly is not a monotonic or symmetrical dependence on sequence position, hence indicating local perturbations in residue mobility.

ST-ESR spectra of the 5-MSL spin-labeled major coat protein mutants in DOPC bilayers at L/P 50 mol/mol are given in Figure 3. With the exception of the mutant A49C, which displays fast motion on the conventional ESR time scale, the spectra are mostly characteristic of relatively rapid motion on the slower ST-ESR time scale (Thomas et al., 1976). The effective rotational correlation time for the spin-labeled major coat protein mutant A25C estimated from calibrations of the diagnostic spectral line height ratios lies between 5 and approximately 10−20 μs for the low-field and high-field regions, respectively (Horváth & Marsh, 1983; Marsh, 1992). This is the mutant that displays little segmental motion on the conventional ESR time scale (see Figures 1 and 2) and therefore is most likely to reflect the overall rotational motion of the whole protein. The effective rotational correlation is defined in terms of isotropically rotating calibration systems.

The T_1 relaxation enhancement by Ni^{2+} ions of spin-labeled mutants, incorporated in DOPC vesicles at L/P 50 mol/mol, is given in Figure 4. All samples were deoxygenated. Effective spin−lattice relaxation times, T_1, were obtained from progressive saturation experiments with increasing microwave power, together with line width measurements, as described under Materials and Methods. The T_1 relaxation rate is found to be directly proportional to the Ni^{2+} ion concentration for all the different spin-labeled mutants in the concentration range 2.5−50 mM $NiCl_2$ (cf. eq 2). The slopes of the concentration dependence of the relaxation rate in Figure 4 are a measure of the accessibility

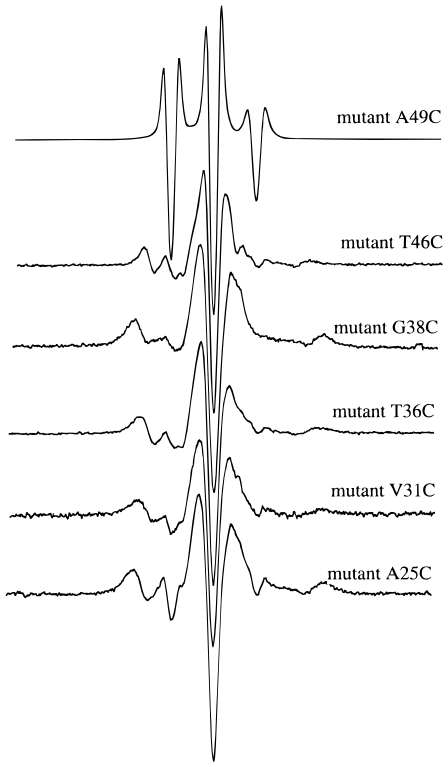

FIGURE 3: Saturation transfer ESR spectra of spin-labeled major coat protein mutants in DOPC bilayers at a lipid to protein ratio of 50 mol/mol. The temperature of the samples is 20 °C. Total scan width is 16 mT.

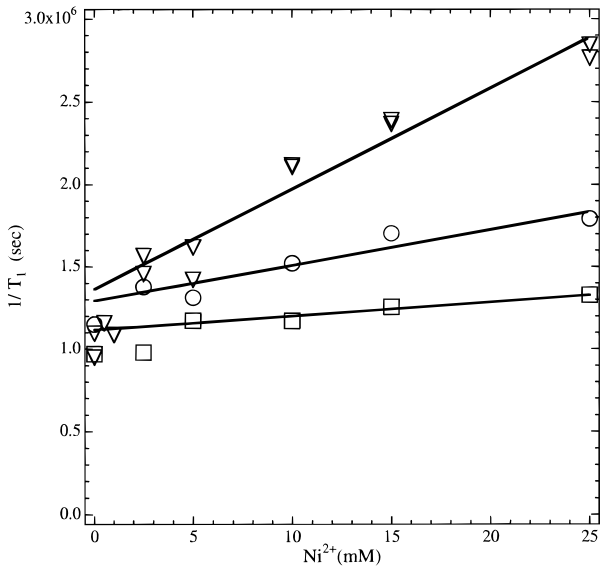

FIGURE 4: Dependence of the reciprocal T_1 relaxation times of the spin-labeled major coat protein mutants reconstituted in DOPC bilayers at 20 °C on bulk Ni^{2+} concentration in the aqueous phase. The solid lines represent linear regressions in the concentration range 2.5−25 mM Ni^{2+}. Data are given for three representative spin-labeled mutants: A49C (triangles), V31C (circles), and G38C (squares).

to aqueous Ni^{2+} ions, or their distance of closest approach, for the different spin-labeled mutant major coat proteins. The relaxation enhancements by Ni^{2+} ions at low concentrations (<2.5 mM) will be considered later. Relaxation enhancements were also determined for samples saturated with oxygen (in the absence of $NiCl_2$), and the accessibilities of the different spin-labeled mutants to oxygen were calculated according to eq 3.

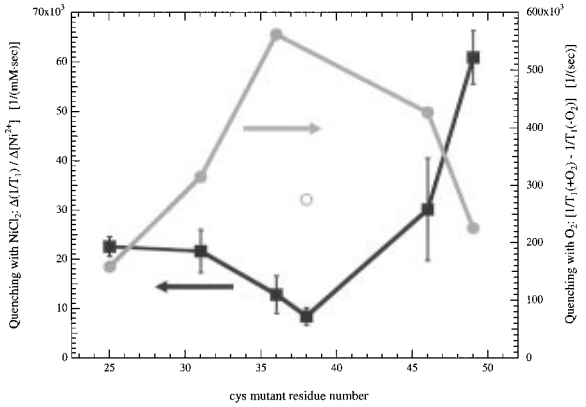

FIGURE 5: Dependence on label position of the relaxation enhancements by oxygen (circles) and by Ni^{2+} (squares) of the spin-labeled major coat protein mutants in DOPC bilayers. The left-hand ordinate (squares) gives the gradient of the increase in spin-label T_1 relaxation rate with respect to Ni^{2+} concentration. The right-hand ordinate (circles) gives the difference in spin-label T_1 relaxation rate for samples saturated with oxygen and deoxygenated samples. The G38C mutant shows a tendency to aggregate, and its accessibility to oxygen is given by the open circle.

The accessibilities both to oxygen and to Ni^{2+} ions that were determined from the relaxation enhancements are given in Figure 5 for the various spin-labeled major coat protein mutants incorporated in DOPC bilayers at L/P 50 mol/mol. The cysteine mutants studied span the hydrophobic as well as the C-terminal domain of the major coat protein. The relaxation enhancement by aqueous Ni^{2+} ions decreases from position 25 to position 38 and then increases steeply to position 49. It should be noted that for spin-labeled residues embedded in the membrane, the relaxation enhancement induced by aqueous Ni^{2+} ions does not represent a direct accessibility but rather a distance-dependent, through-space effect of magnetic dipole interactions (Páli et al., 1992). The results with aqueous Ni^{2+} ions are in contrast to the accessibility to oxygen dissolved in the hydrophobic interior of the membrane. The relaxation enhancement induced by molecular oxygen increases from position 25 to position 36 and then decreases toward position 49. The maximum accessibility to oxygen at position 36 corresponds to the minimum relaxation enhancement by Ni^{2+} ions which occurs around positions 36 and 38. This suggests that this region corresponds to the center of the bilayer membrane.

The asymmetry in the distribution of relaxation enhancements induced by Ni^{2+}, which is strongest in the case of residue 25, suggests that none of the labeled residues on the N-terminal side of the protein (from residue 25 onward) are directly exposed to the aqueous phase. The irregularity in the distribution of accessibility to oxygen, relative to the overall profile, may partly be attributed to sequence/secondary structure-specific effects.

To calibrate the positional dependence of the relaxation enhancements obtained from the spin-labeled protein, comparable experiments were performed with spin-labeled lipids in the presence of oxygen or $NiCl_2$. The relaxation enhancements for a lipid head group spin-label (TS) and for phospholipids spin-labeled in the chain (5-PCSL, 9-PCSL, 14-PCSL) determined in DOPC bilayers with and without the unlabeled major coat protein are given in Figure 6. The relaxation enhancement of the phospholipid spin-labels by both oxygen and aqueous Ni^{2+} ions is modified somewhat by insertion of the major coat protein in the bilayer, but the

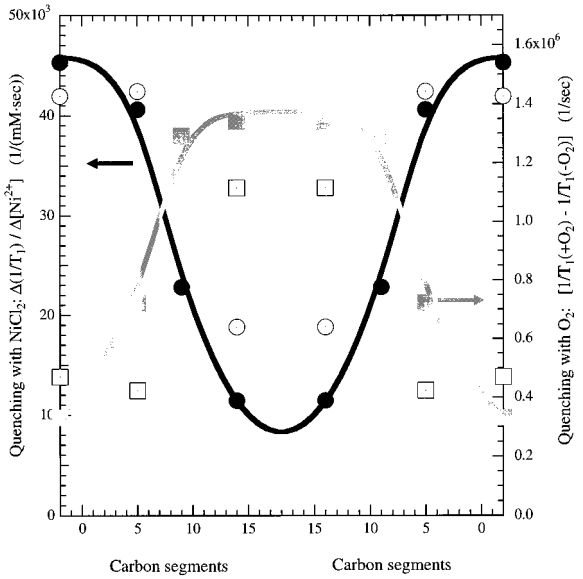

FIGURE 6: Dependence on label position of the relaxation enhancement by oxygen (filled squares) and by Ni^{2+} (filled circles) for the lipid head group spin-label (TS) and for spin-labeled phospholipid acyl chains (5-PCSL, 9-PCSL, 14-PCSL) in DOPC bilayers. The relaxation enhancement of spin-labeled lipids in DOPC bilayers containing unlabeled major coat protein by oxygen is indicated by open circles and by aqueous Ni^{2+} by open squares.

overall positional profiles remain qualitatively the same. The decrease in relaxation enhancement by oxygen of the chain-labeled lipids is probably caused by a decreased solubility of oxygen in the hydrophobic interior of the protein-containing bilayers. This correlates with the decreased chain mobility evidenced by the spectra of the chain-labeled lipids in the presence of protein (data not shown). From Figure 6, it can be seen that the relaxation enhancement by oxygen or by aqueous Ni^{2+} is increasing or decreasing monotonically as a function of the distance from the lipid head group phosphate region. The effect of oxygen is relatively low in the aqueous phase and in the phospholipid head group region, but increases toward the center of the membrane. This is consistent with the known preference of oxygen to dissolve in the hydrocarbon phase.

Compared to oxygen, the relaxation enhancement by aqueous Ni^{2+} ions shows qualitatively the inverse profile with position of the spin-labels in the membrane. Large enhancements induced by Ni^{2+} ions are observed for spin-labels at the membrane surface in the lipid head group region. These then decrease rapidly with depth in the membrane for the chain-labeled lipids because of the diminishing dipolar interactions with Ni^{2+} ions confined to the aqueous phase. Because the bilayers are symmetrical and the *n*-PCSL spin-labels are uniformly distributed, the relaxation enhancements by both oxygen and Ni^{2+} ions represent both halves of the bilayer and are plotted relative to both surfaces of the bilayer in Figure 6.

The relaxation enhancements by aqueous Ni^{2+} ions that are given in Figure 5 were determined for high $NiCl_2$ concentrations (>2.5 mM). However, the concentration dependence was biphasic with a different dependence of the relaxation enhancement by Ni^{2+} ions in the low concentration range of 0−2.5 mM $NiCl_2$ (see Figure 4). This initial relaxation enhancement at low Ni^{2+} ion concentrations is also dependent on the position of the spin-labeled cysteine. The high efficiency of this relaxation enhancement almost

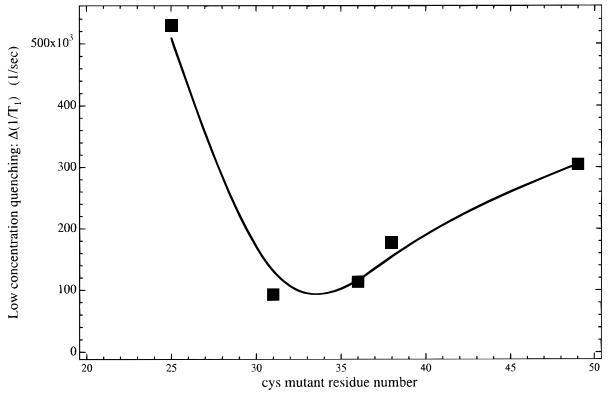

FIGURE 7: Difference in relaxation rates, $\Delta(1/T_1)$, between the linear regression intercepts of the relaxation dependence at high $NiCl_2$ concentrations (2.5−25 mM) and at low $NiCl_2$ concentrations (0−2.5 mM) for different spin-labeled mutant major coat proteins at 20 °C in DOPC bilayers.

certainly arises from binding of Ni^{2+} ions to a specific site on the protein. No biphasic behavior upon $NiCl_2$ titration was observed with the spin-labeled TS or *n*-PCSL lipids (data not shown). The relaxation enhancement of the spin-labeled mutant proteins at low Ni^{2+} concentrations is given in Figure 7. Plotted is the total relaxation enhancement in the low concentration region which is obtained from the difference between the relaxation rate in the absence of $NiCl_2$ and the extrapolated value at zero concentration from the linear regression of the dependence in the high concentration regime. The effect at low Ni^{2+} concentrations is most pronounced for the spin-labeled A25C mutant and sharply decreases for the spin-labeled mutants V31C, T36C, and G38C with an increase again toward the C-terminus.

DISCUSSION

The location of spin-labeled site-directed mutants of the M13 major coat protein reconstituted into DOPC vesicles has been investigated directly by determining the accessibility of the spin-labeled sites to molecular oxygen and to cationic Ni^{2+} ions. In the latter case, a decreasing distance-dependent relaxation enhancement is expected for spin-labeled residues that are embedded in the membrane. The major coat protein mutants were selected to be regularly spaced along the lipid-exposed transmembrane protein surface, almost completely traversing the bilayer.

From the profiles of relaxation enhancement by both oxygen and Ni^{2+} ions (Figure 5), it can be seen that the spin-labeled residue T36C is located near the center of the bilayer. The spin-labeled mutants V31C and G38C are clearly located in the hydrophobic core of the membrane. There is also little doubt about the aqueous location of the spin-label on the A49C mutant, due to its high mobility on the time scale of conventional ESR, the high isotropic hyperfine splitting (1.59 mT), and the respective relaxation enhancements by both oxygen and aqueous Ni^{2+} ions. Such a transmembrane profile is also in agreement with the efficiency of spin-labeling for which the lowest accessibility for alkylation of SH groups by 5-MSL is found with the mutants V31C, T36C, and G38C.

Previously, it was suggested that the transmembrane domain extends toward the C-terminus up to Thr46 (Stopar et al., 1996), leaving the α-carbon of the lysine side chains in the membrane, while the ϵ-amino groups are interacting

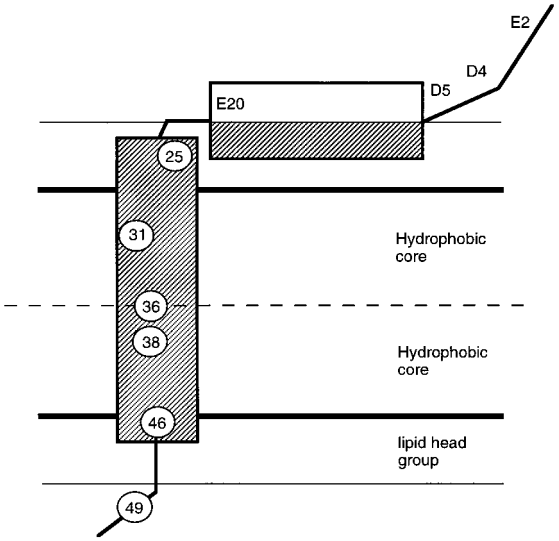

FIGURE 8: Location of the M13 major coat protein in a phospholipid bilayer. The two boxed regions represent a transmembrane helix and an amphiphilic helix aligned along the membrane surface. The residues that were changed to cysteine and spin-labeled are indicated by numbered circles. The positions of the amino acids with spin-labeled side chains are indicated in the amphipathic helix and in the N-terminus. The solid horizontal lines indicate the approximate boundaries of the lipid polar head groups in the bilayer. The dashed line indicates the center of the bilayer.

with the phosphates of the lipid head groups. The nitroxide spin-label covalently attached to the mutant coat protein T46C has a reduced relaxation enhancement by Ni^{2+} ions as compared to A49C, and a significantly increased oxygen accessibility. Relatively high relaxation enhancement by Ni^{2+} does not permit this residue to be buried in the membrane. The rather high oxygen accessibility of this mutant and the reduced mobility on the conventional ESR time scale, on the other hand, suggest that the spin-label attached to T46C is located in a more hydrophobic environment. The accessibility to both polar and apolar relaxants would thus qualitatively locate the spin-label at T46C in the lipid head group region. The exact location of the membrane−water interface in the C-terminal domain of the major coat protein, however, is further complicated by four positively charged lysines intercalated between apolar residues. The relatively high oxygen accessibility could possibly be provided by the glycerol moiety of the lipid head group and the surrounding strongly hydrophobic phenylalanines and leucine residues in the α-helical conformation of the protein. Such a location of the T46C residue is further supported by an independent study using the accessibility of fluorescence-labeled M13 major coat proteins to different fluorescence quenchers (Spruijt et al., 1996).

The relaxation enhancement profiles for both oxygen and Ni^{2+} ions exhibit an asymmetric distribution across the membrane toward position 25 (Figure 5). Additionally, the positional profile of the mobility of the spin-labeled residues that is given in Figure 2 is highly asymmetric. This is not altogether surprising when the asymmetric structure of the major coat protein is taken into account (see Figure 8). The major coat protein in the membrane-bound form consists of two connected helices: a transmembrane and an amphipathic helix that are oriented perpendicular to one another (Nambudripad et al., 1991; Williams et al., 1996). Thermodynamically, the most probable location for the amphipathic helix is aligned along the membrane surface (White & Wimley, 1994). This orientation would determine the position of the interface in the N-terminal section of the transmembrane helix. The spin-label at position 25 is highly immobilized, which may be because it is squeezed between the two helices in the lipid head group region, as has already been proposed (Stopar et al., 1996). Alternatively, the trend to increasing side-chain mobility toward the C-terminal (Figure 2) could suggest that the N-terminal end of the transmembrane helix is preferentially anchored by the surface association of the amphipathic helix to which it is attached. Relaxation enhancement of the spin-labeled A25C mutant by aqueous Ni^{2+} is low, which would locate this residue inside the membrane. However, the low accessibility of this residue to oxygen suggests that it cannot be buried deep in the hydrophobic core. The low oxygen accessibility may arise partly because the spin-label on mutant A25C is spatially constrained between the two helices in the polar head group region. The Ni^{2+} ion distribution on this side of the bilayer may also be complicated by the presence of the charged amphipathic helix at the membrane surface as indicated by low Ni^{2+} concentration relaxation enhancement. The two different mechanisms of spin relaxation enhancement on interaction with fast-relaxing Ni^{2+} ions at low Ni^{2+} concentration and high Ni^{2+} concentration, respectively, may not be directly comparable. High efficiency of relaxation for low Ni^{2+} concentration is attributed to binding of Ni^{2+} ions to the protein; on the other hand, Ni^{2+} ions in the bulk phase are responsible for the high Ni^{2+} concentration relaxation. The bulk Ni^{2+} ion distribution on the spin-labeled A25C mutant coat protein side of the bilayers, however, is complex as discussed above. The exclusion of the bulk Ni^{2+} ions is the main reason for the low apparent accessibility at higher Ni^{2+} concentrations. It is clear from the low accessibility to bulk Ni^{2+} ions, however, that this spin-label cannot be located in the aqueous phase, but it is likely to be positioned in the membrane interfacial region.

The nitroxide spin-label covalently attached to the mutant coat protein G38C shows the smallest relaxation enhancement by Ni^{2+} ions, which is consistent with its location in the hydrophobic core. It is notable, however, that the oxygen accessibility is rather low. This mutant shows a tendency to aggregate by partially forming β-sheet structures. It is therefore possible that oxygen is excluded from collisions with those spin-labels that are tightly packed within the protein aggregate [cf. Altenbach et al. (1990)]. Overall, the asymmetry in the profile of oxygen accessibility (Figure 5) may arise to some extent from local sequence-specific effects such as are evident in the modulation of the increasing side-chain mobility from the N- to the C-terminal in Figure 2. Comparison of these two figures suggests that a locally low mobility (i.e., high value of A_{max}) correlates with a high value of oxygen accessibility and vice-versa. This alternation in ΔA_{max} and $\Delta(1/T_1)$ has a roughly helical periodicity, and examination of a helical wheel reveals clustering of large and hydrophobic side chains close to the face containing spin-labels with high values of A_{max} and oxygen-induced relaxation enhancements. The one exception to this is the low oxygen accessibility of spin-labeled mutant A25C, for which other possible origins have already been discussed.

In general, the relaxation enhancements of the spin-labeled major coat protein mutants by oxygen are lower than those for the calibration set of spin-labeled phospholipids in the hydrophobic region. The two spin-labeled systems may not

be comparable directly in quantitative terms because of the higher mobility of the spin-labeled lipids. However, the 2-fold difference in efficiency of oxygen-induced relaxation suggests that the spin-labeled coat proteins may be associated to some extent in the lipid membranes, hence reducing the accessibility to oxygen. Effective rotation correlation times estimated from isotropic calibrations of the ST-ESR spectra for the mutant that shows the least mobility on the conventional ESR time scale (A25C) are in the region of 5−15 μs. The correlation times for uniaxial rotation, $\tau_{R||}$, are maximally half this value, assuming that the most probable orientation of the spin-label is perpendicular to the rotation axis (Marsh & Horváth, 1989). Hydrodynamic calculations, however, suggest rotational correlation times of $\tau_{R||} \sim 0.1-0.2$ μs for a transmembrane α-helical monomer with membrane viscosities in the range 2.5−5 P (Marsh & Horváth, 1989). Although the rotational diffusion will be further hindered by the surface interactions of the amphipathic N-terminal helix (Wolkers et al., 1997), this comparison suggests that a limited reversible association of the transmembrane helices does occur.

The very efficient relaxation induced by the spin-labeled mutants at low Ni^{2+} concentrations (Figure 4) strongly suggests specific binding of Ni^{2+} to the protein. The enhancement is greatest for the A25C mutant (see Figure 7), which indicates that the metal ion site is situated in the N-terminal domain. There are five negative charges in the major coat protein: four in the N-terminal arm, Glu2, Asp4, Asp5, Glu20, and one at the terminal COOH group. These may act as binding sites for the positively charged Ni^{2+} ions. Estimates of the distance of these sites from the spin-label by using the Solomon−Bloembergen equation [see, e.g., Marsh (1992) and Páli et al. (1992)] give values of ca. 11 Å for the spin-label on mutant A25C and ca. 15 Å for the spin-label on mutant G31C. This would favor Glu20 as being one of the residues associated with Ni^{2+} ion binding. The relatively large enhancement found for the spin-labeled mutant A49C (Figure 7) probably arises from a random transmembrane orientation of the coat protein in the reconstituted membrane. This could allow the C-terminal to come into close proximity at the membrane surface with the N-terminal domain of an adjacent protein.

CONCLUSION

The location of the site-specific major coat protein mutant agents in the phospholipid bilayer, as determined by paramagnetic relaxation, is indicated schematically in Figure 8. Amino acid residues 25 and 46 are located in the lipid head group region at the membrane−water interface. A short part of the C-terminus (three to four amino acid residues) extends into the aqueous phase. This transmembrane topography is in agreement with a parallel study on fluorescence-labeled major coat protein mutants (Spruijt et al., 1996). Such a membrane location inevitably leaves the α-carbons of Lys40, Lys43, and Lys44 in the membrane interior. The distance between residues 25 and 46 is 31.5 Å in an α-helical conformation, which is compatible with the thickness of a DOPC bilayer of 36 Å as measured by X-ray diffraction (Gruner et al., 1988). The location of the Ni^{2+} binding site in the N-terminal amphipathic helix positions this at the membrane surface. Local sequence-specific effects are consistent with the α-helical structure. The lower oxygen accessibility for protein membrane spin-labels compared with the spin-labeled lipids suggests a reversible hydrophobic association of the proteins in the membrane.

REFERENCES

Altenbach, C., Flitsch, L. S., Khorana, G. H., & Hubbell, W. L. (1989) *Biochemistry 28*, 7806−7812.

Altenbach, C., Marti, T., Khorana, H. G., & Hubbell, W. L. (1990) *Science 248*, 1088−1092.

Altenbach, C., Greenhalgh, D. A., Khorana, H. G., & Hubbell, W. L. (1994) *Proc. Natl. Acad. Sci. U.S.A. 91*, 1667−1671.

Asbeck, F., Beyreuther, K., Kohler, H., Wettstein, G., & Braunitzer, G. (1969) *Physiol. Chem. 350*, 1047.

Bales, B. L. (1989) in *Biological Magnetic Resonance−Spin-Labeling Theory and Applications* (Berliner, L. J., & Reuben, J., Eds.) pp 77−130, Plenum Press, New York and London.

Fajer, P., & Marsh, D. (1982) *J. Magn. Reson. 49*, 212−224.

Gruner, S. M., Tate, M. W., Kirk, G. L., So, P. T. C., Turner, D. C., Keane, D. T., Tilcock, C. P. S., & Cullis, P. R. (1988) *Biochemistry 27*, 2853−2866.

Hemminga, M. A., De Jager, P. A., Marsh, D., & Fajer, P. (1984) *J. Magn. Reson. 59*, 160−163.

Horváth, L. I., & Marsh, D. (1983) *J. Magn. Reson. 54*, 363−373.

Hubbell, W. L., Mchaourab, H. S., Altenbach, C., & Lietzow, M. A. (1996) *Structure 4*, 779−783.

Marsh, D. (1981) *Mol. Biol., Biochem. and Biophys., 31* 51−142.

Marsh, D. (1992) *Appl. Magn. Reson. 3*, 53−65.

Marsh, D. (1994) in *Electron Spin Resonance*, *Specialist Periodical Reports* (Atherton, N. M., Davies, M. J., & Gilbert, B. C., Eds.) Vol. 14, pp 166−202, The Royal Society of Chemistry, Cambridge.

Marsh, D. (1995a) *Spectrochim. Acta A51*, L1−L6.

Marsh, D. (1995b) *J. Magn. Reson. A114*, 248−254.

Marsh, D., & Watts, A. (1982) in *Lipid−Protein Interactions (Jost, P. C., & Griffith, O. H., Eds.) Vol. 2, pp 53−156, Wiley-Interscience, New York.*

Marsh, D., & Horváth, L. I. (1989) in *Advanced EPR. Applications in Biology and Biochemistry* (Hoff, A. J., Ed.) pp 707−752, Elsevier, Amsterdam.

Marvin, D. A., Hale, R. D., Nave, C., & Citterich, M. H. (1994) *J. Mol. Biol. 235*, 260−286.

McDonnell, P. A., Shon, K., Kim, Y., & Opella, S. J. (1993) *J. Mol. Biol. 233*, 447−463.

Nambudripad, R., Stark, W., Opella, S. J., & Makowski, L. (1991) *Science 252*, 1305−1308.

Páli, T., Bartucci, R., Horváth, L. I., & Marsh, D. (1992) *Biophys. J. 61*, 1595−1602.

Páli, T., Horváth, L. I., & Marsh, D. (1993) *J. Magn. Reson. A54*, 363−373.

Snel, M. M. E., & Marsh, D. (1993) *Biochim. Biophys. Acta 1150*, 155−161.

Snel, M. M. E., De Kruijff, B., & Marsh, D. (1994) *Biochemistry 33*, 11150−11157.

Spruijt, R. B., Wolfs, C. J. A. M., & Hemminga, M. A. (1989) *Biochemistry 28*, 9159−9165.

Spruijt, R. B., Wolfs, C. J. A. M., Verver, J. W. G., & Hemminga, M. A. (1996) *Biochemistry 35*, 10383−10391.

Stopar, D., Spruijt, R. B., Wolfs, C. J. A. M., & Hemminga, M. A. (1996) *Biochemistry 35*, 15467−15473.

Subczynski, W. K., & Hyde, J. S. (1983) *Biophys. J. 41*, 283−286.

Subczynski, W. K., & Hyde, J. S. (1984) *Biophys. J. 45*, 743−748.

Thomas, D. D., Dalton, L. R., & Hyde, J. S. (1976) *J. Chem. Phys. 65*, 3006−3024.

Turner, R. J., & Weiner, J. H. (1993) *Biochim. Biophys. Acta 1202*, 161−168.

Van de Ven, F. J. M., Van Os, J. W. M., Aelen, J. M. A., Wymenga, S. S., Ramerowski, M. L., Konings, R. N. H., & Hilbers, C. W. (1993) *Biochemistry 32*, 8322−8328.

White, S. H., & Wimley, W. C. (1994) *Curr. Opin. Struct. Biol. 4*, 79−86.

Williams, K. A., Farrow, N., Deber, C. M., & Kay, L. E. (1996) *Biochemistry 35*, 5145−5157.

Wolkers, W. F., Spruijt, R. B., Kaan, A., Konings, R. N. H., & Hemminga, M. A. (1997) *Biochim. Biophys. Acta 1327* (in press).

BI970139V